Realization of an all-optical triode and diode with a two-level-atom–loaded diffraction grating

Richard W. Ziolkowski

A finite-difference time-domain full-wave vector Maxwell equation solver is coupled with a two-level-atom model to simulate the scattering of an ultrafast pulsed Gaussian beam from a finite-length, metallic lamellar grating loaded with two-level atoms. The atomic medium is taken to be resonant at or near the frequency of the incident optical radiation. The highly resonant material and grating behaviors are then combined to realize an all-optical triode at low powers and an all-optical diode at high powers. Simulation results demonstrate the operating characteristics of these triode and diode configurations. © 1997 Optical Society of America

Key words: Optical triode, optical diode, scattering from gratings, ultrafast phenomena.

1. Introduction

All-optical switches are intrinsic components in many potential photonic devices and systems, including those associated with optical communications and computing. There have been many proposals for all-optical switches that utilize material nonlinearities. These include studies of optical diode configurations dealing with linear and nonlinear interfaces (for instance, Refs. 1 and 2). Consider the scattering of a pulsed Gaussian beam that is focused onto a linear–nonlinear interface at an angle beyond the critical angle for the medium. The linear portion of the index of refraction of the nonlinear medium is selected slightly lower than that of the linear medium but with its nonlinear portion able to increase the index above the linear medium's value at some critical value of the incident field intensity. If the incident pulse intensity is below that critical value, the beam senses the interface and experiences a strong (critical) reflection from it. If the pulse intensity is above that critical value, the interface becomes transparent to the beam, and the beam is strongly transmitted into the nonlinear medium. Finite-difference time-domain (FDTD) simulations[3] confirmed the conclusions given experimentally in Ref. 1 and theoretically in Ref. 2 that, in contrast to the plane-wave case, there is simply too much energy leakage into the nonlinear medium from the initial focused pulsed beam components, whose wave vectors are below the critical value for this configuration to have any practical value. These conclusions were further emphasized in Ref. 4, where the results of three-dimensional simulations of a Gaussian beam from a linear–nonlinear interface showed the complex breakup of the reflected and transmitted beams.

The use of gratings in the design of optical switches is common. Recent examples of optically controlled grating switches include using a deep grating in a semiconductor multiple-quantum-well waveguide,[5] a grating-assisted nonlinear coupler as an optical switch,[6] and a second-order grating-coupled surface-emitting laser.[7] There have also been numerous attempts at achieving an optical triode configuration. These include devices based on a nonlinear etalon and gradient index lenses[8,9] and biased quantum-well structures.[10]

I found that the combination of a finite-length, metallic, lamellar grating loaded with a resonant two-level atom material can act as an effective all-optical triode for both low-power cw and ultrafast pulses and as a diode for both high-power cw and ultrafast pulses. To explain the physics underlying the associated small-distance-scale and short-time-scale interactions, particularly in the resonance regime of the materials and the associated device structures, a first-principles, rather than a phenomenological, approach was considered to be the most desirable. As discussed in Ref. 11, this leads to a semiclassical Maxwell–Bloch model, i.e., a careful marriage between microscopic (quantum-mechanical) material

The author is with the Electromagnetics Laboratory, Department of Electrical and Computer Engineering, University of Arizona, Tucson, Arizona 85721.

Received 9 June 1997.
0003-6935/97/338547-10$10.00/0

models of the resonant material systems and the macroscopic Maxwell's equation solver.

The two-dimensional FDTD Maxwell–Bloch simulator is briefly introduced in Section 2. The concepts that define the optical triode and diode configurations are introduced in Section 3. The numerical simulation results are discussed in Section 4. Conclusions are given in Section 5.

2. Finite-Difference Time-Domain Simulator

The optical triode and diode switching effects associated with the scattering of a focused, pulsed Gaussian beam from a grating loaded with two-level atoms were investigated with a multidimensional generalization of the FDTD Maxwell–Bloch simulator introduced in Ref. 11. To simplify the analysis, I consider the *s*-polarization (electric field polarized along the edges of the corrugations in the grating) case. This model requires the numerical solution of the two-dimensional TE Maxwell–Bloch system.

TE Maxwell equations.

$$\partial_t H_x = +\frac{1}{\mu_0}\,\partial_z E_y, \tag{1a}$$

$$\partial_t H_z = -\frac{1}{\mu_0}\,\partial_x E_y, \tag{1b}$$

$$\begin{aligned}\partial_t E_y &= \frac{1}{\epsilon_0}\,(\partial_z H_x - \partial_x H_z) - \frac{1}{\epsilon_0}\,\partial_t P_y \\ &= \frac{1}{\epsilon_0}\,(\partial_z H_x - \partial_x H_z) - \frac{N_{\text{atom}}\gamma}{\epsilon_0 T_2}\,\rho_1 + \frac{N_{\text{atom}}\gamma\omega_0}{\epsilon_0}\,\rho_2.\end{aligned} \tag{1c}$$

Bloch equations.

$$\partial_t \rho_1 = -\frac{1}{T_2}\,\rho_1 + \omega_0\rho_2, \tag{1d}$$

$$\partial_t \rho_2 = -\omega_0\rho_1 - \frac{1}{T_2}\,\rho_2 + 2\,\frac{\gamma}{\hbar}\,E_y\rho_3, \tag{1e}$$

$$\partial_t \rho_3 = -2\,\frac{\gamma}{\hbar}\,E_y\rho_2 - \frac{1}{T_1}\,(\rho_3 - \rho_{30}), \tag{1f}$$

where T_1 is the excited-state lifetime, T_2 is the dephasing time, and ρ_{30} is the equilibrium population difference in the system. The dispersive or in-phase component of the polarization, the absorptive or in-quadrature component of the polarization, and the fractional difference in the populations for the two energy levels are represented by the terms ρ_1, ρ_2, and ρ_3, respectively. The number of atoms per unit volume is N_{atom}; the dipole coupling coefficient of the two-level atom is γ. The corresponding macroscopic polarization field $\mathbf{P}(x, z, t) = -N_{\text{atom}}\gamma\rho_1(x, z, t)\hat{y}$. Note that the specification that $\rho_3(t = 0) = \rho_{3i} = -1$ $(+1)$ represents all the atoms' initially being in their ground (excited) states. In all the simulations considered below, the equilibrium population difference was fixed at $\rho_{30} = -1.0$.

I find that the FDTD predictor–corrector scheme introduced in Ref. 11 also satisfactorily handles this more complicated two-dimensional nonlinear system of equations. The FDTD approach can handle ultrafast single-cycle pulse cases as readily as multiple-cycle cases that have an intrinsic carrier wave, and it can incorporate complicated scatterers and materials with great flexibility.

The proposed configuration is shown in Fig. 1. I used a perfectly conducting metallic grating for the current study to simplify the analysis; more realistic metals can[12,13] and will be included in future simulations. The length of a unit cell of the grating is L; the depth of this corrugation is h; and the duty factor is a/L, where a is the length of the metal region in the unit cell. The complementary region in a unit cell is filled with a material composed of uniform, two-level atoms. The cases discussed below use either 11 or 19 unit cells in the grating structure. The pump beam of the triode would be provided either by an ultrafast pulsed Gaussian beam normally incident upon the grating or by an ultrafast pulsed beam that is in line with the corrugations of the grating (i.e., along the $\hat{y}$ direction). The pump beam would control the initial population difference ρ_{3i} of the two-level atom material. As shown in Ref. 11, specified values of ρ_3 can be achieved, even with a single-cycle pump pulse. I obtained the optical triode and diode simulations without this pump beam by simply setting ρ_3 to a specified level ρ_{3i} at $t = 0$. The normally incident pump beam can be included in future simulations, if desired, to help improve the design of this configuration.

The space above the grating is split into two regions, I and II, their interface coinciding with the normal to the grating, which is located at the center of the material portion of the cell at the center of the grating. The point of intersection between this interface and the surface of the grating is the location of the focal center of the input beam. The input beam (probe beam) is incident upon the grating from region II at an angle θ_{inc}. It is launched from a total-field–scattered-field interface (Ref. 14, p. 111) located 5.62 wavelengths away from the grating. The input power in the probe beam, S_{in}, is measured in the total field region by calculation of the integrated Poynting's flux (the total amount of power) radiated into the total field region. The output of this device is measured in the scattered-field region by calculating the integrated Poynting's flux radiated separately into regions I and II. The integrated output power reradiated into regions I and II is denoted, by S_1 and S_2, respectively. The differential scattering factor,

$$S = \frac{(S_1 - S_2)}{(S_1 + S_2)}, \tag{2}$$

is a measure of the amount of power scattered into one region versus the other. It is positive (negative) if the power scattered into region I is larger (smaller)

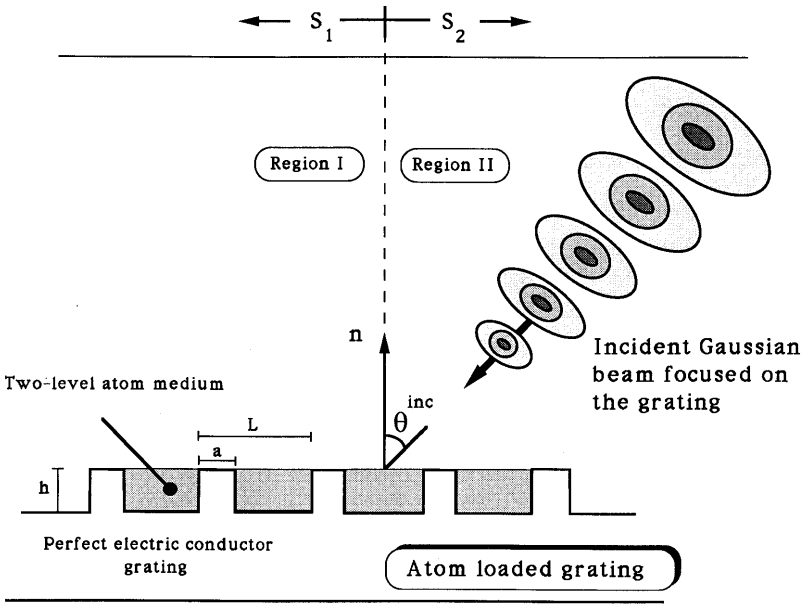

Fig. 1. Basic simulation geometry for a two-level, atom-loaded diffraction grating illuminated with a pulsed Gaussian beam that can act as an optical triode or diode. These optical triode and diode configurations were studied with a two-dimensional FDTD Maxwell–Bloch simulator.

than the power scattered into region II. The output of the optical triode is selected to be forward (negative) biased when the beam scatters into region II (I). The weighted differential output

$$\mathrm{WDO} = -S\,\frac{S_2}{S_{\mathrm{in}}}, \tag{3}$$

then couples the gain of the output beam, i.e., the beam scattered into region II, to the differential scattering factor. The negative sign compensates for the fact that S is negative when a major portion of the output beam scatters back into region II.

The entire far-field scattering pattern can be obtained from the near-field FDTD simulation results by use of recently developed near-to-far-field transform methods.[12–16] The electric- and magnetic-field components are recorded at points in a specified plane. These time histories are used to define equivalent time-dependent infinitesimal magnetic and electric currents. A Fourier transform of these currents leads to their equivalent frequency-domain dipole radiators. The radiation pattern is obtained from a sum of the far fields radiated by all of these dipoles.

The predictor–corrector scheme was set to perform five iterations for each time step to minimize the run times of the simulations. Testing with more iterations per time step produced no significant variations in the results. The meshes consisted of 400×1200 cells, and the simulations were run for either 3000 or 6000 time steps. The discretization in all the two-dimensional runs was taken to be $\lambda/50$; those simulations were run at the two-dimensional Courant limit to minimize the number of time steps. A 10-cell Berenger PML (Ref. 13, p. 181) absorbing boundary condition was used to truncate the FDTD mesh. The FDTD simulations of the optical triode and diode configurations were run on a Digital Equipment Corporation ALPHA 6/300 workstation running at 333 MHz. The two-dimensional runs with 3000 time steps took ~20 min to complete.

3. Loaded Grating Optical Triode and Diode

To understand the possible switching effect that combines the grating phenomena with the nonlinear, two-level, atom medium, I consider the one-dimensional Maxwell–Bloch equations obtained from Eqs. (1) ($H_z = 0$ with the electric field polarized along the y axis) in the limit that the level transition angular frequency ω_0, i.e., $E_{g\to e} = \hbar\omega_0$, the excited state lifetime T_1, and the dephasing time T_2 satisfy $T_2 \ll T_1$, $\omega_0 T_1 \gg 1$, and $\omega_0 T_2 \gg 1$. In addition, I consider low-amplitude beams so that the Rabi frequency $\omega_{\mathrm{Rabi}} = 2\gamma|\mathbf{E}|/\hbar$ satisfies $\omega_{\mathrm{Rabi}} \ll \omega_0$. With these assumptions the one-dimensional Maxwell–Bloch equations (1) yield the relations

$$\partial_z{}^2 E_y - \partial_{ct}{}^2 E_y = \mu_0 \partial_t{}^2 P_y \approx N_{\mathrm{atom}} \gamma \mu_0 \omega_0{}^2 \rho_1, \tag{4a}$$

$$\partial_t{}^2 \rho_1 + \omega_0{}^2 \rho_1 = -\frac{1}{T_1}\,\partial_t \rho_1 - \frac{\omega_0}{T_2}\,\rho_2 + 2\,\frac{\gamma}{\hbar}\,E_y \omega_0 \rho_3$$

$$\approx 2\,\frac{\gamma}{\hbar}\,E_y \omega_0 \rho_3, \tag{4b}$$

where $\partial_{ct} = c^{-1}\partial_t$. These relations mean that the susceptibility in the frequency domain χ_ω for this medium has the form

$$\chi_\omega \approx -\rho_3 \Lambda \left[1 - \left(\frac{\omega}{\omega_0}\right)^2\right]^{-1}, \tag{5a}$$

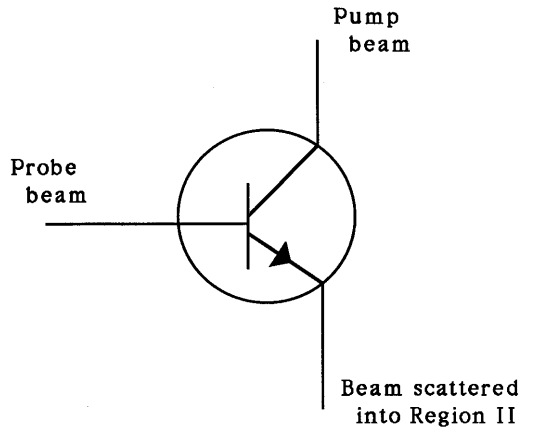

Fig. 2. Equivalent transistor schematic of the optical triode.

where

$$\Lambda = \frac{2N_{\text{atom}}\gamma^2}{\hbar\omega_0\epsilon_0}. \tag{5b}$$

Let the angular frequency of the electromagnetic wave ω be near the resonance frequency so that $\omega = \omega_0(1 + \delta)$. Relation (5a) then yields

$$\chi_\omega \approx +\rho_3 \frac{\Lambda}{2\delta}. \tag{6}$$

The corresponding index of refraction for this medium is $n(\omega) = (1 + \chi_\omega)^{1/2}$. Thus, if the incident wave has its frequency slightly above the resonance frequency so that $0 < \delta \ll 1$ and if the ratio $\Lambda > 2\delta$, then the two-level medium becomes reflecting or penetrable depending on whether ρ_3 is negative or positive, respectively. Therefore, if the atoms are in their ground (excited) state, the medium acts as a plasma below (above) cutoff. If the incident field has a small amplitude and a pulse duration $T_p \ll T_1$, there is only a slight variation in ρ_3 during the time of interaction of the beam with the atoms; therefore $\rho_3(t) \approx \rho_{3i}$. Consequently, one can control χ_ω by controlling ρ_{3i}.

However, it is well known that, by selecting a grating structure appropriately, one can control the direction in which the scattered beam propagates. These preferred directions are determined by the phase-matching condition

$$\sin\theta_{\text{out}} = \sin\theta_{\text{inc}} + m\frac{\lambda}{n(\omega)L}, \qquad m = 0, \pm1, \pm2, \ldots, \tag{7}$$

where θ_{inc} and θ_{out} are the incident and output angles, respectively, measured with respect to the normal to the grating. If the grating is then loaded with atoms satisfying the parameter constraints dictated above, it could be made to switch the direction of the scattered beam, depending on the value of ρ_{3i} because that parameter controls the susceptibility and hence the index of the medium between the grating teeth. If $\rho_{3i} = -1.0$ and the atoms are in their ground state (triode-off state), the index is negative and the atom-loaded grating acts as a reflector. The incident pulsed beam in this case interacts with the atom-loaded grating, but it does not penetrate into the regions between the grating teeth. Hence the beam specularly reflects from the atom-loaded grating essentially unchanged. However, with $\rho_{3i} = +0.10$, for example, the atoms are partially excited and the beam now penetrates into the region between the teeth. The output beam direction is then determined by the Bragg condition [Eq. (7)] and is affected somewhat by whatever effective index of refraction is realized

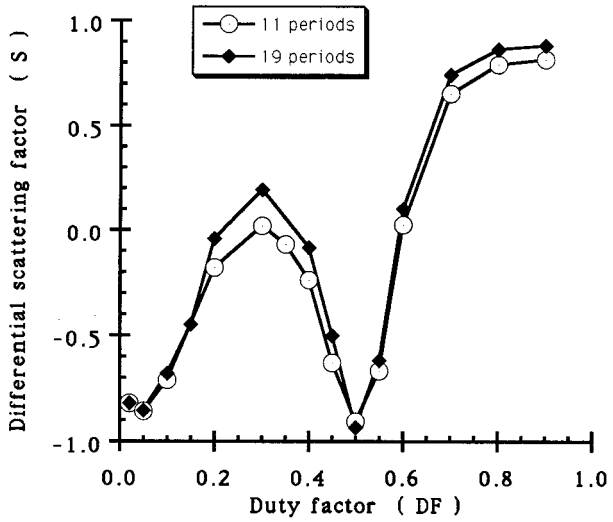

Fig. 3. Unloaded grating used to design the structure selected for the optical triode and diode studies. The resulting differential scattering factor is shown for several values of the duty factor for one grating with 11 unit cells and one with 19 unit cells.

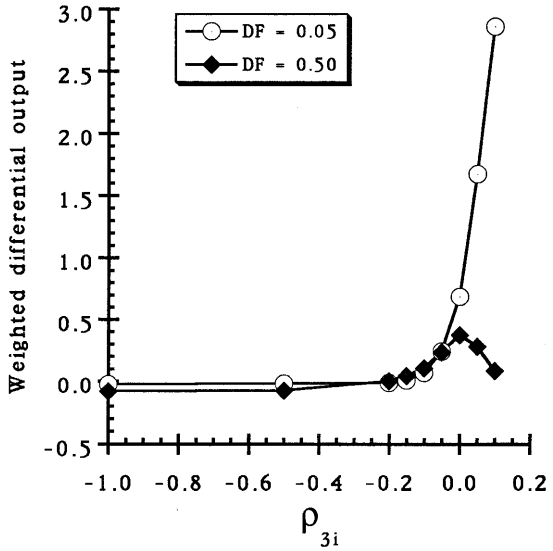

Fig. 4. Weighted differential output obtained as a function of the initial population difference ρ_{3i} for optical triode configurations with a grating of 11 unit cells and duty factors DF = 0.05 and DF = 0.50.

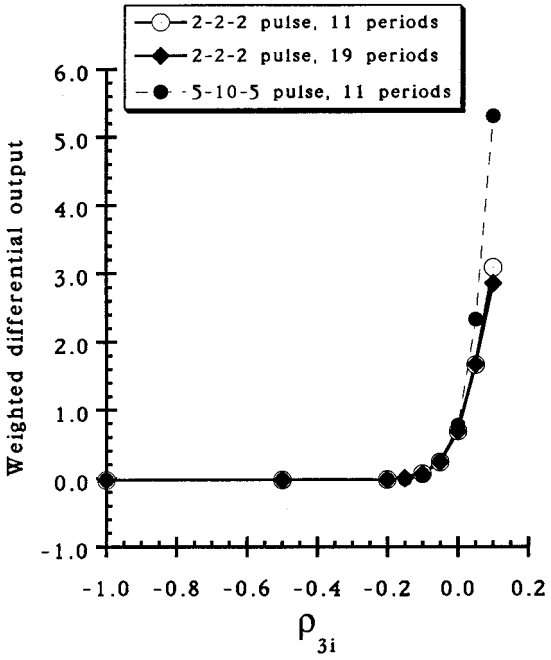

Fig. 5. Weighted differential output obtained as a function of the initial population difference ρ_{3i} for optical triode configurations with ○, an 11-unit-cell grating and the 2–2–2 incident pulse; ◆, a 19-unit-cell grating and the 2–2–2 incident pulse; and ●, an 11-unit-cell grating and the 5–10–5 incident pulse. The duty factor of the grating was DF = 0.05 for all of these cases.

with the atom loading. Moreover, as with any grating application, the allowed number of diffraction orders can be controlled by a careful selection of the grating period L. Additionally, as shown in Ref. 10, when the atoms are initially in their excited state and the incident beam is at low power, the two-level atom system should act as a gain medium and could be coaxed into transferring its energy to the field. This two-level-atom-loaded grating could thus lead to an all-optical triode.

The optical triode concept is shown in Fig. 2 in terms of a (n-p-n small-signal amplifier) transistor diagram. The pump beam, which controls the number of excited atoms and hence ρ_{3i}, acts as the collector. It provides the energy for the amplification process. The input or probe beam represents the gate signal. The shape or modulation of the input pulse controls the modulation of the output beam. The beam scattered from the grating then represents the output or emitter signal.

The response time of the triode is controlled by the length of the incident pump and probe beams. As demonstrated in Ref. 10, the pump beam can be a large-amplitude, single-cycle (ultrafast) pulse. The probe beam can be an ultrafast pulse (the cases considered below include six-cycle and 20-cycle optical pulses). Thus the proposed all-optical triode can operate in the femtosecond regime.

For a high-power incident beam one would expect a different mode of operation. Consider all the atoms to be in their ground state so that $\rho_{3i} = -1.0$. A large-amplitude, high-power beam, i.e., a beam with $\omega_{\mathrm{Rabi}} \sim \omega_0$, can stimulate many of the atoms into their excited state. One might expect, for these high powers, that the resulting ρ_3 value for the atoms in one of the waveguides or cavities formed by one of the corrugations in the grating could be approximately zero, i.e., equal amounts of the atoms are found in their ground and in their excited states. The loaded grating then acts as though it were not loaded because $\chi_\omega \sim 0$. If the grating were designed to scatter the output beam with negative S values when it was not loaded and with positive S values for $\rho_{3i} = -1.0$ at low powers

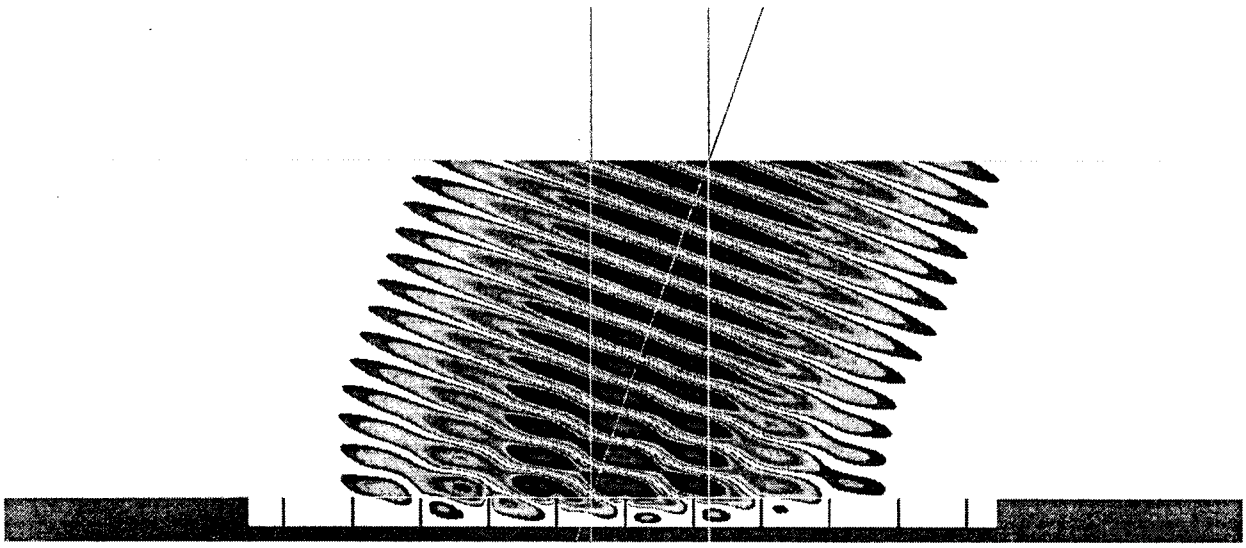

Fig. 6. FDTD incident 5–10–5 pulse electric-field distribution at the exact time that the beam interacts with the atom-loaded diffraction grating of duty factor DF = 0.05. The angle of incidence is 19.5°. The additional lines depict the beam-center line, the normal to the grating at the point where the beam center strikes the grating, and the normal to the grating that intersects the total-field–scattered-field source boundary at the initial beam center.

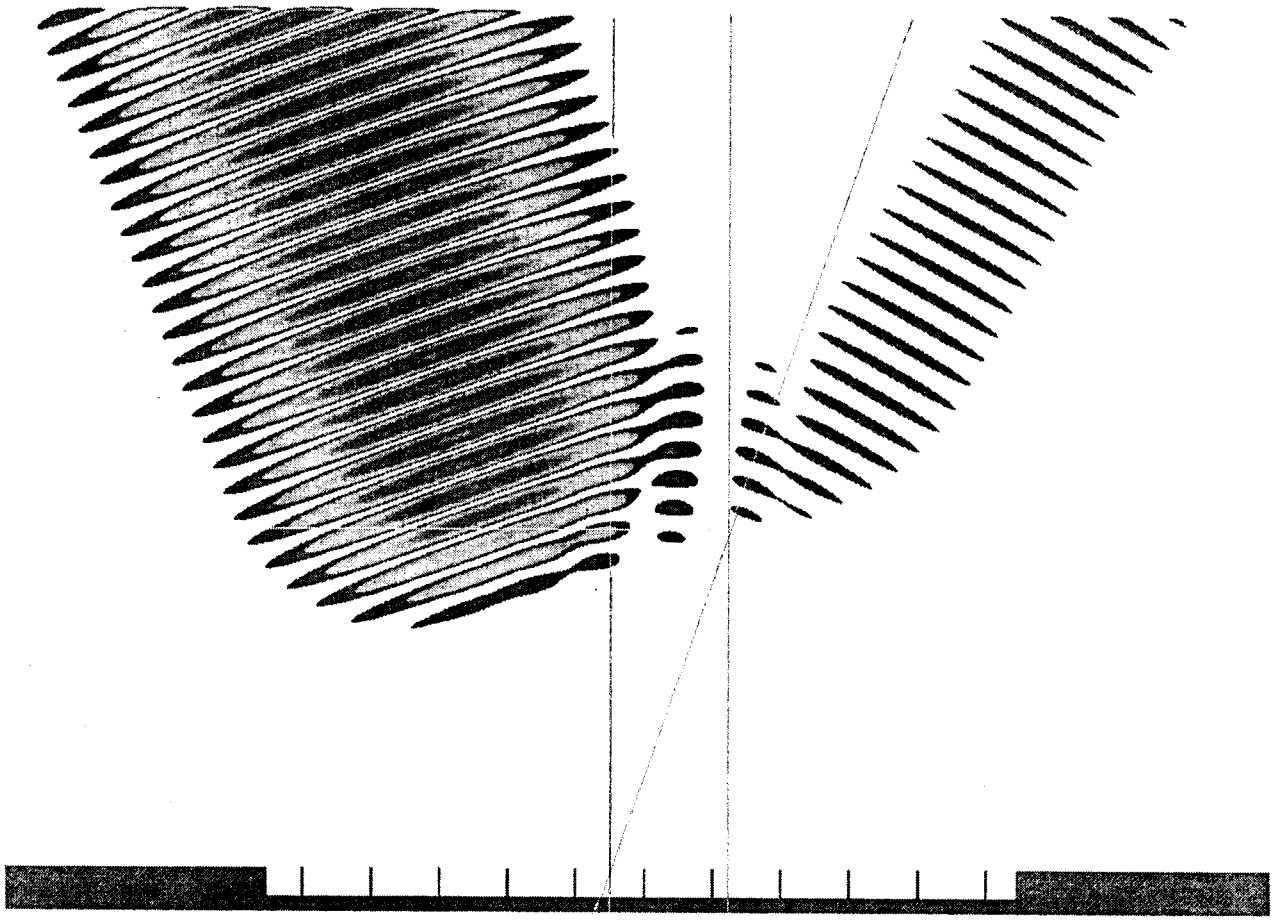

Fig. 7. FDTD scattered field distribution at a time after the entire 5–10–5 incident pulse given in Fig. 5 has interacted with the atom-loaded grating. The atoms are initially in their ground state characterized by $\rho_{3i} = -1.0$. The pulsed beam has been reflected by this grating, with only minor distortion.

when it was loaded, the loaded grating would switch from negative to positive values of WDO as the power was increased. Thus the loaded grating acts as a diode based upon the maximum amplitude of the incident beam.

4. Finite-Difference Time-Domain Simulation Results

The first step in this proof-of-concept design process was to determine the combination of the grating parameters that provides the lowest and highest possible values of S for an unloaded grating. This was accomplished by running the FDTD simulator with the two-level atom solver turned off. The basic beam parameters were selected to be similar to those used in previous FDTD simulations of several periodic and aperiodic grating structures and optical storage disks.[11,12] The FDTD method accurately predicted the scattering response in all of those cases.[11,12]

The grating parameters were chosen to be $L = 1.17$ μm and $h = 0.50$ μm. Two gratings, one with 11 unit cells and one with 19 unit cells, were used. An $f = 3.1415 \times 10^{14}$ Hz (0.955-μm wavelength) windowed sinusoidal Gaussian beam with a waist of 2.925 μm = 3.063λ was incident upon the grating at $\theta_{inc} = 19.5°$. For an infinite grating these parameters allow only the −1 and 0 beam orders to exist in the scattered beam according to the Bragg relation, Eq. (7). These grating parameter specifications also resulted in the Gaussian beam waist's being $2.5L$. The amplitude of the incident beam thus reached its e^{-2} point at $5.0L$, a distance almost equal to half the length of the 11-unit-cell grating and a little less than half of the half-length of the 19-unit-cell grating. The incident pulse was a unit-amplitude, 20-cycle, windowed sine wave with five cycles used to turn on the pulse smoothly and five cycles to turn it off in the same manner. This pulse has a narrow frequency spectrum centered on f; it is essentially a monochromatic signal. The input power S_{in} of this 5–10–5 pulse was measured along a line in the total field region that was parallel to the total-field–scattered-field boundary and 10 cells away from it. The output powers S_1 and S_2 were measured along their respective half-lines in the scattered field region; these half-lines were parallel to the total-field–scattered-field boundary and 10 cells away from it. The remaining parameter of the grating, the duty factor (DF), was then allowed to vary, and the resulting differential scattering factor S was measured. The FDTD sim-

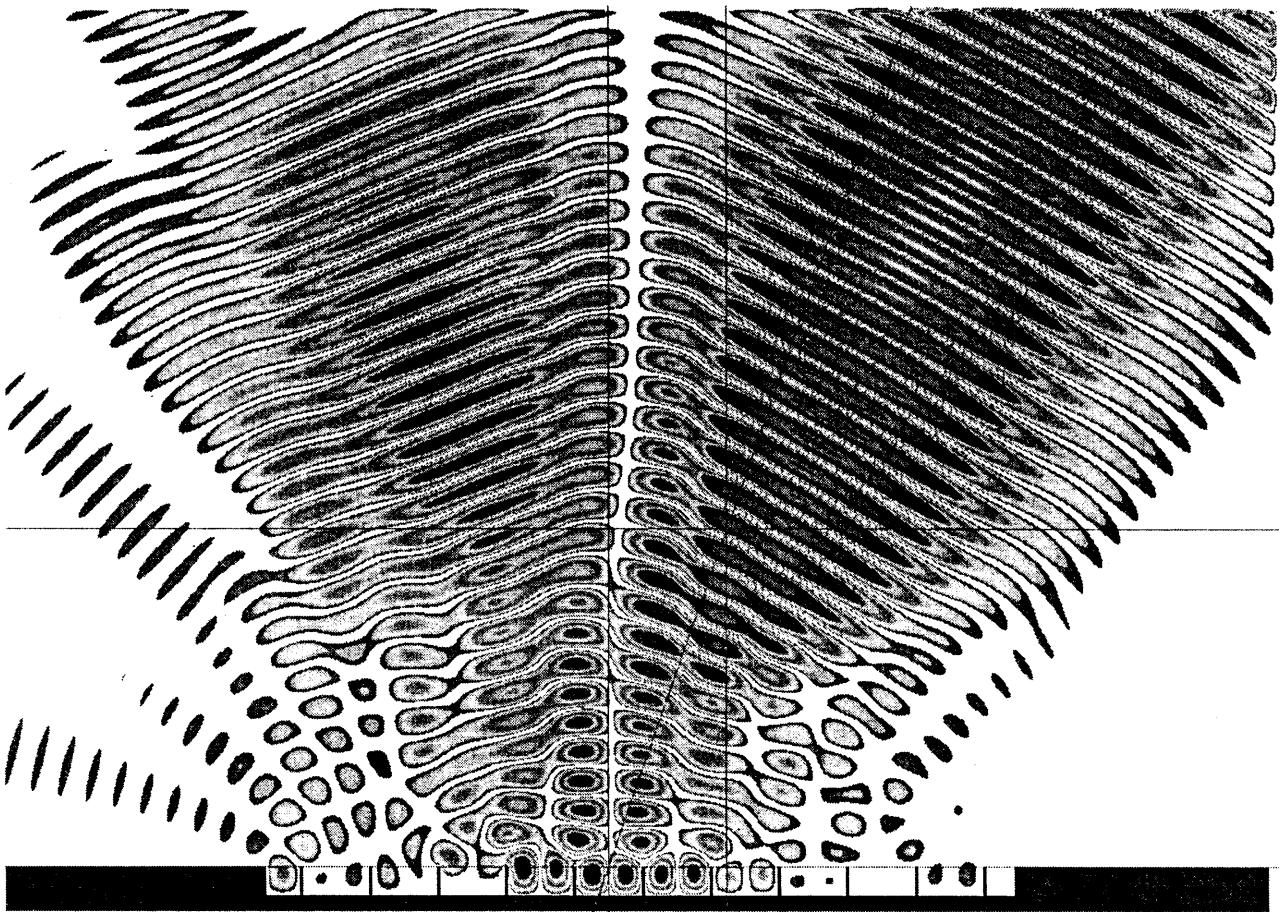

Fig. 8. FDTD scattered field distribution at a time after the entire 5–10–5 incident pulse given in Fig. 5 has interacted with the atom-loaded grating. The atoms are initially in the excited state characterized by $\rho_{3i} = +0.10$. The pulsed beam has been reflected strongly back into the source direction. Some of the beam leaves the grating in the reflected field direction.

ulation results are shown in Fig. 3. The performances of the 11- and the 19-unit-cell gratings were nearly identical; this was a result of the localization of the focused incident-beam energy to the middle 11 cells of the 19-unit-cell grating. The largest responses back into region II occurred near the duty factors DF = 0.05 and DF = 0.50. Either choice would provide the desired forward bias direction; both were investigated as the operating point for the optical triode.

The loaded grating results were obtained with the two-level-atom parameters $\gamma = 1.0 \times 10^{-27}$, $T_1 = 1.0 \times 10^{-10}$ s, and $T_2 = 2.0 \times 10^{-15}$ s. Thus the relaxation time of the atoms was much longer than the pulse duration, while the dephasing time was shorter than it. The two-level atoms loading the grating are taken to have an initial state ρ_{3i} and an equilibrium state $\rho_{30} = -1.0$. A large value for the number of atoms, $N_{\text{atom}} = 1.0 \times 10^{24}$, and a small difference between the transition frequency and the beam frequency, $f_0 = 0.99f$, were selected. This choice of N_{atom}, combined with the parameter $\delta = (f/f_0) - 1 \approx 0.01$ in relation (6), gives $\Lambda/2\delta = 54.2$, a value sufficiently large to achieve the desired optical triode and diode conditions. The choice for the maximum incident field amplitude was $E_{\max} = 1.0$ so that the Rabi frequency ω_{Rabi} was small. In all cases the results are given in terms of the weighted differential output [Eq. (3)] versus the initial population difference ρ_{3i}.

The first comparison, which is summarized in Fig. 4, concerns the 11-unit-cell grating with DF = 0.05 and DF = 0.50. The incident ultrafast pulse was a unit-amplitude, six-cycle, windowed sine wave with two cycles used to turn on the pulse smoothly and two cycles to turn it off in the same manner. This 2–2–2 pulse has a relatively large bandwidth. Figure 4 clearly demonstrates that the loaded grating with DF = 0.05 can act as an optical triode. However, the loaded grating with DF = 0.50 fails to achieve the desired gain situation; it simply does not have enough atoms present to provide the enhanced output. Notice that the value of ρ_{3i} stops at 0.10 in the DF = 0.05 case. The output beam quality deteriorates rapidly beyond this value because so many atoms are stimulated to emit their radiation that the coherence effect caused by the proper phasing of the incident beam and the grating is reduced substantially. The radiation process is no longer collective between each cell of the grating; the atoms in a cell emit in all directions without a strong knowledge of the presence of the grating. Extremely high gain is achieved at a

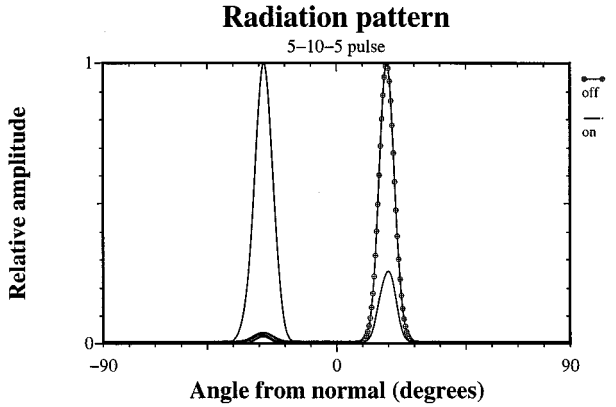

Fig. 9. Normalized far-field radiation pattern generated from the near-field FDTD data obtained when the 5–10–5 incident pulse is scattered from the triode configuration given in Fig. 5, when the triode is off (circled curve), which is characterized by $\rho_{3i} = -1.0$, and when it is on (solid curve), which is characterized by $\rho_{3i} = +0.10$. Positive (negative) angles correspond to a direction of propagation into region I (II). These radiation patterns clearly demonstrate that the grating-based triode acts as a high-fidelity switch for narrow-bandwidth incident pulses.

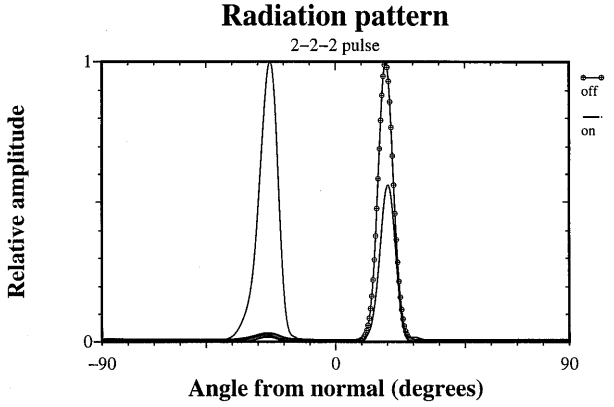

Fig. 10. Normalized far-field patterns generated by the scattering of the 2–2–2 incident pulse from the triode configuration given in Fig. 5 obtained when the triode is both off (circled curve) and on (solid curve). Positive (negative) angles correspond to a direction of propagation into region I (II). These radiation patterns clearly demonstrate that the grating-based triode acts as a reasonably high fidelity switch, even for ultrafast, wide-bandwidth incident pulses.

cost of the beam quality. This response corresponds to the breakdown region of the triode.

The second comparison is summarized in Fig. 5. The performance of the triode is presented for the 2–2–2 pulse with a grating of 11 unit cells, the 2–2–2 pulse with a grating of 19 unit cells, and the 5–10–5 pulse with a grating of 11 unit cells. The duty factor for each of these gratings was fixed at DF = 0.05. Because of the number of cycles in the 20-cycle, 5–10–5 incident pulse, the data points in that case represent the average power through the output surfaces. It was found that the output pulse shape closely followed the input pulse in all of these cases; thus the output of the optical triode maintained the modulation of its inputs.

As expected, the quality of the output beam for the 2–2–2 pulse, 19-unit-cell grating is slightly better than the corresponding 11-unit-cell grating case, but there is no significant variation in the WDO because most of the beam energy is concentrated within the middle 11 cells of the grating. Also, as expected, the 5–10–5 pulse produced a slightly higher gain. This pulse has a longer interaction time with the loaded grating, and hence the corresponding scattered beam acquires more energy from the atoms. More atoms would be needed to produce the same amount of output power for the 2–2–2 input pulse.

To determine the effect of the atom-loaded grating on the quality of the scattered beam, I obtained snapshots in time of the near-field field distributions (i.e., those within the simulation region) and the radiation patterns with the FDTD simulator. The electric-field distribution generated by the FDTD simulator for the 5–10–5 pulse incident upon the 11-cell, atom-loaded grating whose duty factor was DF = 0.05 is shown in Fig. 6. This snapshot was taken at the time just when the incident beam begins to interact with the atom-loaded diffraction grating. The angle of incidence of the incident beam is $\theta_{\text{inc}} = 19.5°$. The additional lines in Fig. 7 are included for references. They depict the beam-center line, the normal to the grating at the point where the beam center strikes the grating, and the normal to the grating that intersects the total-field–scattered-field source boundary at the initial beam center. With the atoms initially in their ground state, i.e., $\rho_{3i} = -1.0$, the resulting scattered electric-field distribution is shown in Fig. 7 after the entire 5–10–5 incident pulse has interacted with the atom-loaded grating. The pulsed beam has clearly been reflected by this grating, with only minor distortion. The electric-field distribution for the corresponding case in which the atoms are initially in a partially excited state with $\rho_{3i} = +0.10$ is given in Fig. 8. The pulsed beam has clearly been reflected strongly back into the source direction, while some of the beam leaves the grating in the reflected field direction.

The amount of distortion that the output beam has actually experienced in the $\rho_{3i} = +0.10$ case cannot be properly ascertained from the near-field electric-field distribution shown in Fig. 8. The interference patterns created by the atom-loaded grating are simply too complex to extract the desired information. Thus the near-field field distributions give an incomplete representation of how effectively the atom-loaded grating acts as a switch. The desired figure of merit can be obtained by augmenting this near-field information with the far-field radiation patterns. In particular, the normalized far-field radiation patterns corresponding to Figs. 7 and 8 are given in Fig. 9. The pattern generated when the triode is off ($\rho_{3i} = -1.0$) is represented by the curve with circles; the pattern generated when the triode is on ($\rho_{3i} = +0.10$) is represented by the solid curve. Positive (negative) angles correspond to a direction of

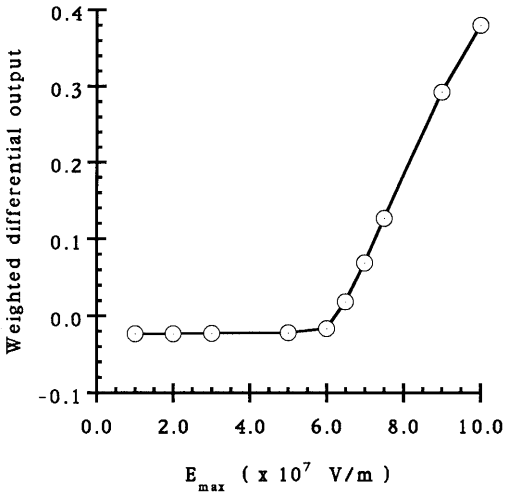

Fig. 11. Weighted differential output obtained as a function of the maximum amplitude $E_{\max}$ of the incident field for the optical diode configuration with the 2–2–2 incident pulse and a 11-unit-cell grating having a duty factor DF = 0.05.

propagation into region I (II). These radiation patterns clearly demonstrate that the grating-based triode acts as a high-fidelity switch for narrow-bandwidth incident pulses and indicate that the beam integrity is quite high, despite the appearance of the near-field distributions. The corresponding radiation patterns for the triode with the same configuration but with the 2–2–2 incident pulse are given in Fig. 10. While the isolation between region I and region II is not as high as it is in the 5–10–5 pulse case, these radiation patterns clearly demonstrate that the atom-loaded grating acts as a reasonably high-fidelity switch, even for ultrafast, wide-bandwidth incident pulses.

The high-power input pulse case is shown in Fig. 11. The grating had 11 unit cells and duty factor DF = 0.05. The input beam was the 2–2–2 pulse. The initial population difference was set to $\rho_{3i} = -1.0$. The maximum amplitude of the pulse $E_{\max}$ varied from 1.0×10^7 to 1.0×10^8 V/m. The expected optical diode behavior was observed. The output beam clearly switched from region I back to region II at the higher power levels. The threshold amplitude was $\sim 6.0 \times 10^7$ V/m, which corresponds to a Rabi frequency $\omega_{\text{Rabi}} = 0.576\omega_0$, a value slightly higher than half of the transition frequency. Close examination of the population difference showed that ρ_3 remained close to its initial value ρ_{3i} during the simulation time until that amplitude threshold was surpassed. With the larger-amplitude incident pulses the population difference was quickly driven into a level near to the value $\rho_3 = 0.0$ and was maintained at that level for the duration of the pulse. The rate of this transition increased proportionally to the amplitude of the incident pulse; more energy was scattered into region II when this transition occurred faster, because the beam was interacting with an effectively unloaded grating for a longer time period. Eventually this process has to saturate at higher values of $E_{\max}$ leaving WDO near 1.0. One can see this starting to occur in Fig. 11; the value of WDO is beginning to taper off at the highest initial field amplitudes.

5. Conclusions

An FDTD simulator that solves the two-dimensional Maxwell–Bloch system of equations was introduced and used to investigate optical triode and diode configurations that are based on a grating loaded with two-level atoms. Switching, amplification, and modulation were demonstrated. Optical triode results were obtained for low-power input beams; optical diode results were obtained for high-power input beams.

I am continuing these design studies of the proposed optical triode and diode configurations. I am considering variations in the waist of the incident beam, the grating shape, the spatial distribution of the atoms in the grating, etc., to determine their optimal operating characteristics. Despite the computational expense associated with these FDTD simulations, they are an efficient approach for these very complex design studies. The pulse properties, grating configurations, and medium dynamics can all be investigated visually and quantitatively in one computing environment. As the optimal operating characteristics of the optical triode and diode become more well understood, the design of a verification experiment will begin.

The author expresses special thanks to Mark Neifeld, Department of Electrical and Computer Engineering, University of Arizona, for his thoughts on an earlier version of this manuscript. This research was supported in part by the U.S. Office of Naval Research under grant N0014-95-1-0636 and by the U.S. Air Force Office of Scientific Research, Air Force Materiel Command, USAF, under grant F49620-96-1-0039.

References

1. P. W. Smith, W. J. Tomlinson, P. J. Maloney, and J.-P. Hermann, "Experimental studies of a nonlinear interface," IEEE J. Quantum Electron. **QE-17,** 340–348 (1981).
2. W. J. Tomlinson, J. P. Gordon, P. W. Smith, and A. E. Kaplan, "Reflection of a Gaussian beam at a nonlinear interface," Appl. Opt. **21,** 2041–2051 (1982).
3. R. W. Ziolkowski and J. B. Judkins, "Applications of discrete methods to pulse propagation in nonlinear media: self-focusing and linear-nonlinear interfaces," Radio Sci. **28,** 901–911 (1993).
4. D. R. Andersen and J. J. Regan, "Reflection and refraction of a three-dimensional Gaussian beam at a nonlinear interface," J. Opt. Soc. Am. A **6,** 1484–1492 (1989).
5. Y. Shibata, M. Ikeda, K. Nakashima, T. Tamamura, and T. Nishida, "Optically-controlled grating switch (OG-SW)," Electron. Lett. **27,** 246–247 (1991).
6. B. E. Little, "Optical-induced spectral tuning in grating-assisted nonlinear couplers," J. Lightwave Technol. **12,** 774–783 (1994).
7. M. H. Shih, F. S. Choa, G. J. Simonis, T. Tanbun-Ek, R. A. Logan, and W. T. Tsang, "Optically controlled surface-emitting beam switches," in *Conference on Lasers and Electro-Optics*,

Vol. 15 of 1995 OSA Technical Digest Series (Optical Society of America, Washington, D.C., 1995), pp. 67–68.
8. H. Tsuda and T. Kurokawa, "All-optical triode device design using a nonlinear etalon and GRIN lenses," Appl. Opt. **29,** 5054–5059 (1990).
9. H. Tsuda and T. Kurokawa, "Construction of an all-optical flip-flop by combination of two optical triodes," Appl. Phys. Lett. **57,** 1724–1726 (1990).
10. M. Yamanishi, "Ultrafast optical processes in DC-field biased quantum well structures," Trans. Inst. Electron. Inf. Commun. Eng. **J74C-I**(11), 449–457 (1991).
11. R. W. Ziolkowski, J. M. Arnold, and D. M. Gogny, "Ultrafast pulse interactions with two-level atoms," Phys. Rev. A **52**(4), 3082–3094 (1995).
12. J. B. Judkins and R. W. Ziolkowski, "Finite-difference time-domain modeling of nonperfectly conducting metallic thin-film gratings," J. Opt. Soc. Am. A **12,** 1974–1983 (1995).
13. J. B. Judkins, C. W. Haggans, and R. W. Ziolkowski, "Two-dimensional finite-difference time-domain simulation for rewritable optical disk surface structure design," Appl. Opt. **35,** 2477–2487 (1996).
14. A. Taflove, *Computational Electrodynamics* (Artech House, Norwood, Mass., 1995).
15. M. J. Barth, R. R. McLeod, and R. W. Ziolkowski, "A near and far-field projection algorithm for finite-difference time-domain codes," J. Electromagn. Waves Appl. **6,** 5–18 (1992).
16. R. Luebbers, K. S. Kunz, M. Schneider, and F. Hunsberger, "A finite-difference time-domain near zone to far zone transformation," IEEE Trans. Antennas Propagat. **AP-39,** 429–433 (1991).